Proceedings World Geothermal Congress 2026
Calgary, Canada, June 8 – 11, 2026

# Modeling of Reservoir Stimulation for Energy Storage in Deep Hydraulic Fractures

Mauricio A. Rivas*, Douglas Simpkins, Victoria McGuire and Lev Ring
Sage Geosystems
mauricio.rivas@sagegeosystems.com

**Keywords:** Pressure-propped fractures, deep downward fractures, energy storage, Huff-n-Puff operations

**ABSTRACT**

Pressure-propped fractures, defined as hydraulic fractures that are maintained open only by fluid pressure without the use of proppants, have been used by (1) the GeneSys Project in Germany (2003 – 2011) for geothermal energy extraction (for district heating); (2) Quidnet Energy (2021) for mechanical energy storage in *shallow* hydraulic fractures; and (3) Sage Geosystems (2023) for mechanical energy storage in *deep* hydraulic fractures. Although similar in form, the three systems have fractures that are created differently, and they employ variants of Huff-n-Puff techniques for their respective energy production. This paper analyzes reservoir stimulations for energy storage in *deep* hydraulic fractures. The systems in mind are where hydraulic fractures on a single wellbore are pressure-propped and only a fraction of the fluid stored in the created hydraulic fracture is cycled via Huff-n-Puff operations. The analysis is done in the more general setting of *downward propagating fractures* that are opposite to the well-studied *buoyant* (or upward) *propagating fractures,* so the language already established there is used here. Attention is given to the hydromechanical dynamics that occur when creating these deep hydraulic fractures; these dynamics are interpreted from the fracture geometries and characteristics resulting from specific stimulation. The open-source solver *PyFrac* is used for the simulations, and different configurations are considered here that are relevant for energy storage in deep hydraulic fractures as well as heat-extraction systems.

## 1 INTRODUCTION

The state of stress of rock formations (in petroleum, geothermal or naturally occurring activities) can vary greatly from homogeneous systems dominated by a near constant stress gradient to stratified systems where different layers above and below the target zone have larger stress magnitudes and/or different rock properties. Several works, such as Adachi et al. (2007), Salimzadeh et al. (2019), Salimzadeh et al. (2020a) and Ghassemi and Kumar (2023), have modeled how changes in the *in-situ* confining stress, as well as fracturing fluid and rock properties, influence the shape of hydraulic fractures that are created in these formations. Knowledge of fracture shapes/geometries resulting from reservoir stimulations is crucial for operations whether it be for oil & gas extraction (Economides and Nolte 2000), heat extraction (Tischner et al. 2013, Fei et al. 2023, Fu et al. 2024, and Tounsi et al. 2025), or mechanical energy storage (Bunger et al. 2023 and Simpkins et al. 2023).

In many cases, such as when fracturing with only water in deep normally faulted regions, a fracture initially propagating radially will tend to grow upwards when buoyant forces become dominant. Möri and Lecampion (2022) analyzed the more general setting of this transition from radial to buoyant elongating fractures and accounted for viscous and toughness competing forces as well as long-term behavior. The effects of stress barriers and fracture toughness on fracture shape were then investigated by Möri, Peruzzo, Garagash, and Lecampion (2024). These two works presented scaling-based arguments that they validated using the open-source boundary element solver *PyFrac*; the solver is documented in Zia and Lecampion (2020) and is based on the implicit level set algorithm (ILSA) developed by Peirce and Detournay (2008). Recently, the morphology of multiple buoyant hydraulic fractures simultaneously propagating from the same horizontal wellbore in formations with near homogeneous confining stress was studied by Möri, Dontsov, and Lecampion (2025). In that study, the authors used the commercial software *Resfrac* for modeling, and geothermal wells motivated their study as fracture shape influences connectivity between two wellbores as used in traditional Enhanced Geothermal Systems (EGS).

In the current work, the *PyFrac* solver is used to investigate how stimulating reservoirs by injecting fluids of density greater than 2 SG affects the shape of the *downward fractures* created. The intended use of these created fractures is for mechanical energy storage systems, or if temperatures are hot enough these may be used for heat extraction systems that are alternative to traditional two-wellbore EGS designs. These subsurface systems are based on fractures that need only connect to a single wellbore, therefore connectivity (to multiple wellbores) issues due to fracture shapes are not studied here. As the studied systems are based on the Huff-n-Puff approach and fractures are maintained open only by fluid pressure during operations, the stimulations modeled do not use/focus on proppant transport/distribution as in Salimzadeh et al. (2020a) or Dontsov and Peirce (2014). Instead, both footprints and widths, with respect to the point of injection of the downward fractures created are considered as these factors have implications for mechanical energy storage and/or heat harvesting strategies in formations that may be layered. The focus in this paper is on the more general setting of *downward fractures* and their hydromechanical dynamics (interpreted from their fracture shapes), so that the analysis here is complementary to that of *buoyant fractures*.

Previous works on downward fractures have been motivated by, for example, the disposal of nuclear waste and other types of hazardous waste. A theory on the related so-called *gravity fractures*, was given by Garagash and Germanovich (2014); see also the related modeling by Salimzadeh et al. (2020b). In a different area, the natural question on the depth of penetration of water-filled crevasses in a glacier was investigated by Weertman (1973). It is worth noting that an early model to calculate the shape of a magma-driven (hence, buoyant) fracture was first given by Weertman (1971). For a review on the development of modeling buoyant fractures see the discussions given by Dahm (2000), Möri et al. (2022) and Möri et al. (2024); for lab testing of downward and buoyant fractures see Taisne and Tait (2009); and for the comparison of laboratory fracture shapes and pressures against predicted numerical work see Jeffrey and Bunger (2009). A study using fiber optic field data to infer hydraulic fracture geometries and capture the continued upward growth is given by the analysis of Bourne et al. (2021).

## 2 METHODOLOGY

The fracture shapes, specifically the footprints and widths, that result when heavy fracturing fluids are used to stimulate formations that may have stress barriers are investigated in this paper. The three types of formations investigated have a minimum *in-situ* stress profile, in the depths of interest, that either (1) has a constant stress gradient, (2) includes a soft stress barrier, or (3) includes a strong stress barrier, delineated by local gradients as defined next.

Assuming a normally faulted formation, a *soft stress barrier* is defined here as a formation depth interval in which the local minimum *in-situ* stress gradient is larger than the specific weight of the fracturing fluid, but not by an order of magnitude or higher (Subsection 3.2 gives an example). A *strong stress barrier* is defined as a depth interval in which the local minimum *in-situ* stress gradient is about one order of magnitude or larger than the specific weight of the fracturing fluid (Subsection 3.3 gives an example). Note that these definitions are dependent on both the formation and fracturing fluid, so that a depth interval that is classified as a strong barrier with respect to one heavy fracturing fluid may be classified as a soft barrier when a much heavier fracturing fluid is used instead.

The open-source 3D planar hydraulic fracture simulator *PyFrac* is used for the numerical simulations of these downward fractures in homogeneous or stratified formations. It should be noted that improvements to *PyFrac* have been made by Peruzzo, Lecampion and Zia (2021), but the results presented here use the code as described in the original documentation by Zia and Lecampion (2020). The solver considers hydraulic fracturing as a coupled physics problem comprising fluid flow and pressure inside the fracture, deformation of the surrounding medium due to the fracture, and propagation of the fracture's tip into the unfractured medium. For these three physics, an implicit finite volume scheme is used for the corresponding elastohydrodynamic lubrication equation, the discretization of the elasticity equation is performed using piecewise constant rectangular displacement discontinuity elements, and the solver combines the discretization of a finite domain with the steadily moving plane-strain hydraulic fracture asymptotic solution near the fracture front. Various implementations of the simulator have shown that the solver is both accurate and robust; see the literature review from their original documentation as well as that in Peruzzo et al. (2021), Möri et al. (2022) and Möri et al. (2024) for solver validation.

## 3 SIMULATION CASES, RESULTS, AND DISCUSSION

A formation, with normal faulting, in which the hydraulic stimulation with a heavy fluid occurs at a true vertical depth (TVD) of 2865 meters is considered for the modeled cases. The profiles of the confining stresses that are used for each of the cases are given in Figure 1. As the intended use of these created fractures is for mechanical energy storage systems, a zero leak-off assumption is made for the simulations.

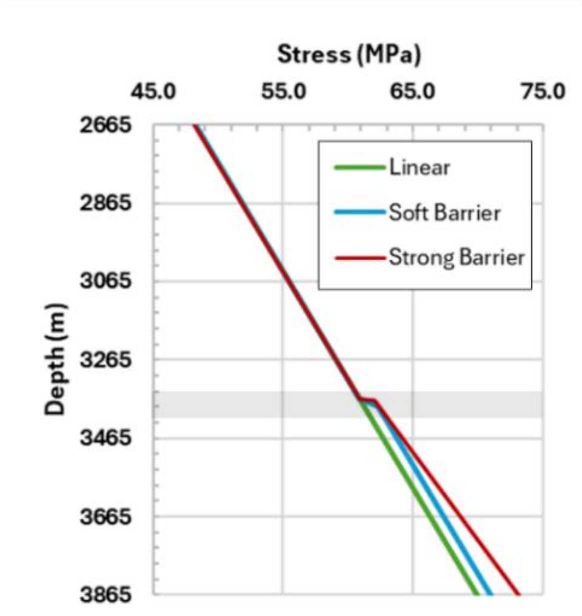


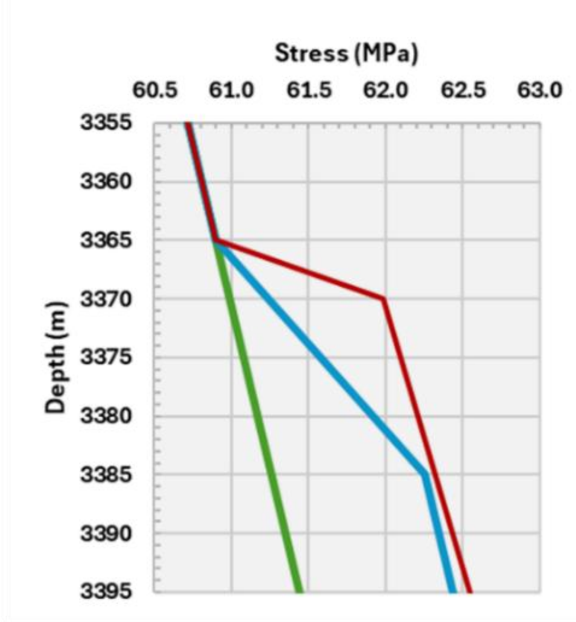


**Figure 1. Profiles of minimum *in-situ* confining stress used in the simulations (left) with a zoomed-in view of the stress barriers (right); note that the soft/strong labels are relative to the fracturing fluid used.**

Möri et al. (2024) indicate that stress barriers on the order of 1 MPa are sufficient for containing *buoyant* hydraulic fractures. Here, we examine the barriers (defined by local stress gradients and the heavy fluid used) and their effect on *downward-propagating* fractures. In particular, we compare the resulting fracture shapes due to the absence/presence of increases of about 1 MPa over specific depth intervals when fracturing with the same 2.4 SG heavy fluid, where the specific weight of the heavy fluid and local stress gradient are both expressed in the same units of psi/ft for consistency. As the transition from radially propagating to buoyant elongating fractures was already analyzed using the *PyFrac* solver in Möri et al. (2024), only the final fracture shapes of these *downward* fractures are captured here. Although stratified formations are much more complex, with each layer having distinct properties such as elastic moduli, toughness, permeability, and porosity, to simplify the analysis, the cases assume the modeled region has homogeneous rock properties. The material properties and operational parameters used for the cases modeled are given in Table 1.

**Table 1. Material properties used for stimulating with a dense fluid.**

| Variable | Unit | Value |
|---|---|---|
| Injection rate | bpm | 42 |
| Fluid density | $\mathrm{kg/m^3}$ | 2400 |
| Fluid viscosity | cP | 24 |
| Poisson's ratio | - | 0.25 |
| Young's modulus | GPa | 33 |
| Fracture toughness | $(\mathrm{MPa}\cdot\sqrt{m})$ | 1 |

### 3.1 Downward Fracturing in a Linear Stress Regime

Consider first injecting a heavy fluid for 2.5 hours into a region (with parameters as in Table 1) where the minimum *in-situ* confining stress follows the *Linear* profile shown in Figure 1 that has a gradient of 0.8 psi/ft in the modeled region. The specific weight (mass density times gravity) of the heavy fluid in the units used here is 1.04 psi/ft, so that by the definitions given above there are no soft nor strong stress barriers in this case (this is intuitively obvious, but we shall use this later). The shape of the induced fracture, at the end of the simulation, is shown in Figure 2 with coordinates relative to the point of injection.

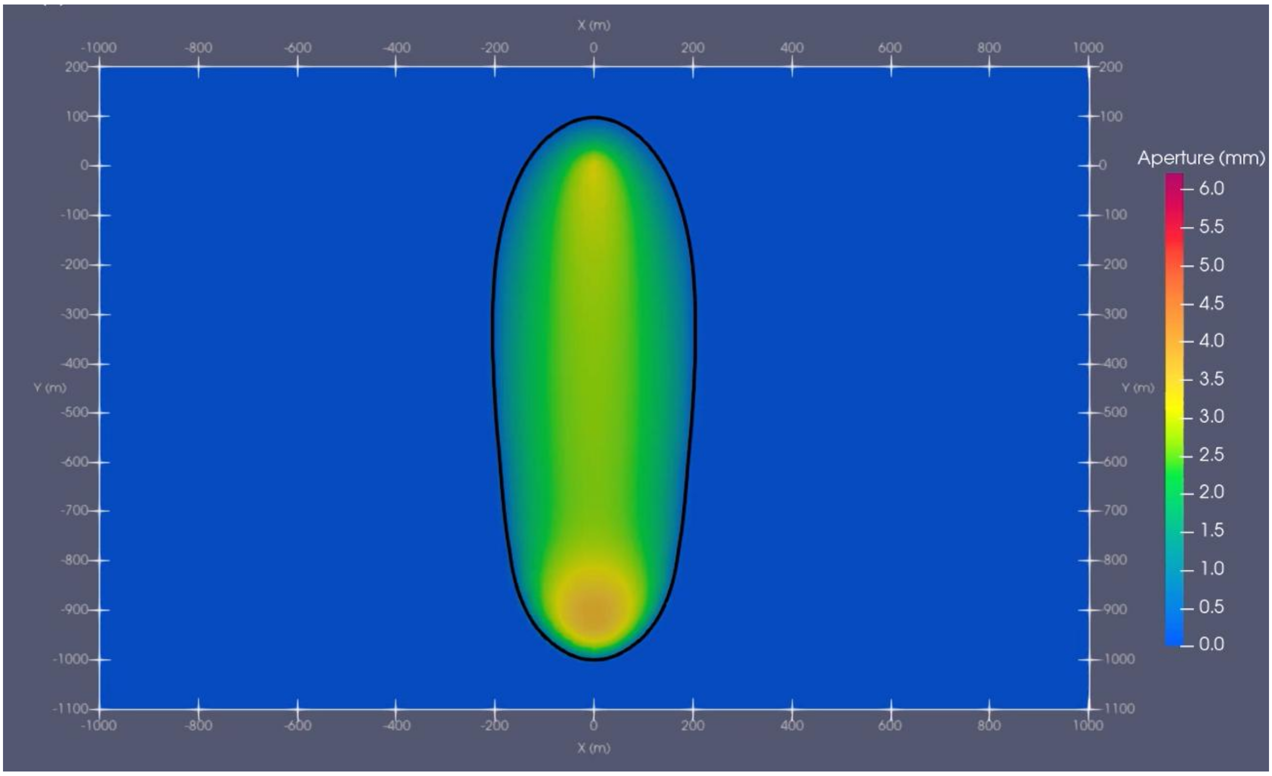


**Figure 2. Shape of the downward fracture that encounters no stress barriers.**

Since the specific weight of the heavy fluid is greater than the confining stress gradient, the fracture prefers to go down when sufficient fluid is injected. This downward fracture then reaches a 1 km distance below the injection point after 2.5 hours of injection. Both around the injection point and in the *head* of the fracture (fracture region below -800 m in Figure 2) the widths are larger than in the rest of the body of the fracture, with larger widths seen in the head. Also seen in the figure is a channel region, called the *tail* of the fracture, between the source region and the head of the fracture where the widths are lower than in the source and head regions but higher than the remaining body of the fracture. The lateral extent (distance in the $x$-direction in the plot), called the *breadth*, of the downward fracture is not uniform due to the fracture toughness assumed, and is slightly larger nearer the source region than in the head.

We point out that the shape of the fracture in Figure 2 will change whether the injection continues or stops at 2.5 hours. If injection continues, the fracture will reach deeper depths but will have a similar shape; if injection stops one needs to also account for the fluid in the wellbore and the ensuing dynamics after shut-in. Hence, merely using zero for the injection rate after 2.5 hours in the solver is not sufficient for a proper modeling. Here, we only report the shape of fractures at the specified instance (2.5 hours in this first case) since we use the hydraulic fracturing *PyFrac* solver as is, i.e. without any modifications or additions, for this short study.

### 3.2 Downward Fracturing through a Soft Stress Barrier

Now consider injecting the same heavy fluid at the same TVD but assume that the confining stress has a change in stress gradient 500 meters below the point of injection (that is, assume the *Soft Barrier* profile in Figure 1) and that the injection is for 4.25 hours. In this second case, the stress increases by 1.4 MPa over the longer distance of 20 meters, so that the *local* stress gradient has gradually increased from 0.8 psi/ft to 3 psi/ft. Since the local stress gradient (3 psi/ft) in this 20-meter formation depth interval is larger than the specific weight of the heavy fluid (1.04 psi/ft), but not by an order of magnitude or higher, this 20-meter interval is classified as a *soft stress barrier* according to the definition given above.

Note that if a 10 SG fluid is considered (as in nuclear waste disposal processes, which is not our focus of study), the 20-meter depth interval will not be considered a soft barrier or a barrier at all since, in this case, the corresponding specific weight of the 'fluid' (ignoring any cement mixture) would be 4.34 psi/ft which is larger than the local stress gradient (3 psi/ft). We thus emphasize that the classifications of barriers depend on both the local stress gradients and on the specific weight of the fracturing fluid utilized.

For the soft stress barrier case, the shape of the induced downward fracture at the end of the 4.25-hour simulation is shown in Figure 3. The shape of this fracture at 2.5 hours is somewhere between that seen in Figure

3 and that shown in Figure 4 in the next subsection, with an appreciable penetration into the layer below the soft stress barrier in this second case. We discuss next only the resulting fracture shape at hour 4.25.

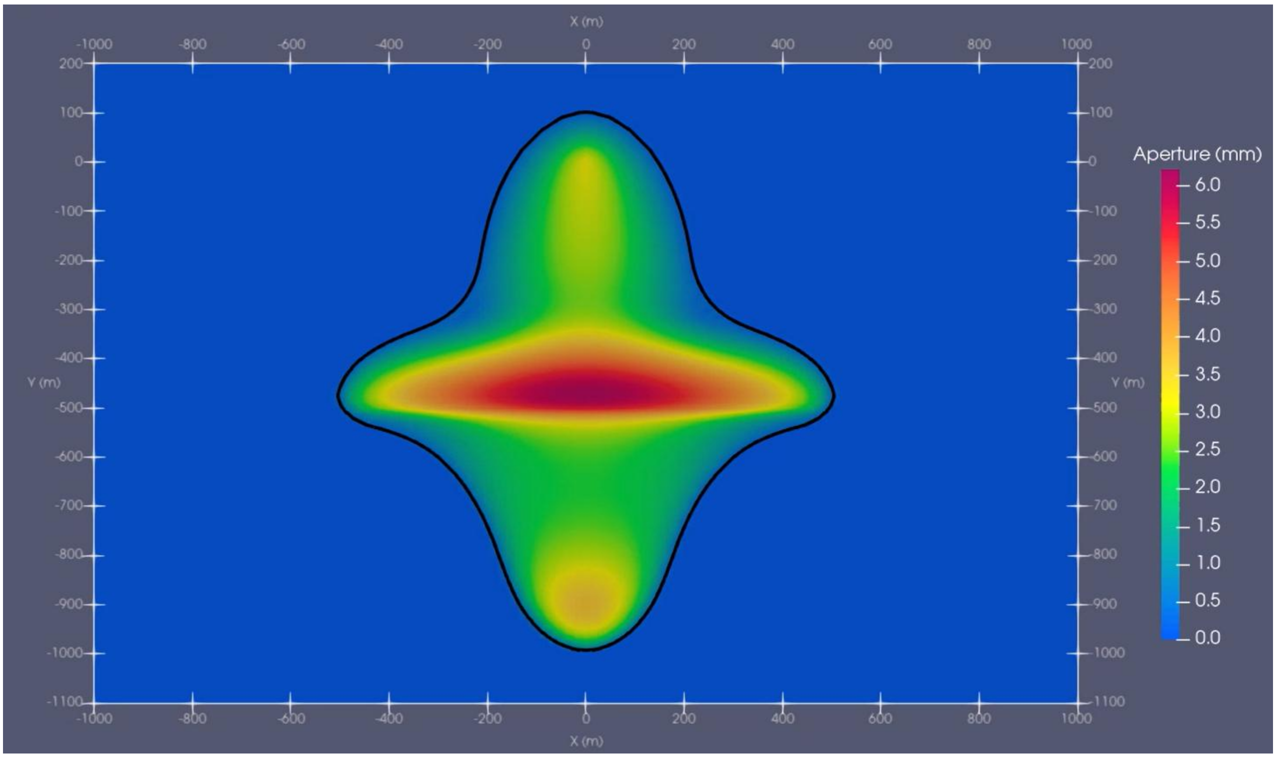


**Figure 3. Shape of downward fracture that passes a soft stress barrier.**

As in the previous case, the high specific weight of the heavy fluid leads to preferential downward growth for the fracture after sufficient fluid has been injected. However, when the downward fracture penetrates the stress barrier, the local confining stress gradient here is greater than the specific weight of the heavy fluid as stated above. Consequently, the fracture prefers to grow laterally (that is, in the $x$-direction) in a somewhat height-contained fashion, but we record here that the fracture does continue to penetrate past the barrier and into the lower rock layer after 2.5 hours. For the downward fracture to reach a 1 km distance below the injection point, the operation needs to continue for about 4.25 hours. Therefore, in the case of a soft stress barrier, it is possible for downward fractures to achieve 1 km distances.

As seen in the figure, the soft stress barrier significantly changes the shape of the fracture created in 4.25 hours. The region near but mainly above the stress barrier, called the *interaction region*, has the greatest widths that are twice as much as those found in the source region or in the head of the fracture. There is a channel between the source and interaction regions with greater widths than in the channel between the interaction and head regions. Both channels have smaller widths than in the source or head regions, but bigger widths than in the remaining body of the fracture outside the interaction region.

In general, the breadth (or lateral extent) of the downward fracture is larger than in the case of a constant stress gradient throughout the entire depths modeled. Due to the soft stress barrier reducing the downward velocity of the fracture, the breadth becomes further elongated in the interaction region as some fluid accumulates in and above the soft stress barrier. In the depth interval corresponding to the channel between the source and interaction regions, the resulting breadth is larger than in the first case since the (lateral, but more so the upwards) growth of the interaction region consequently grows the breath of this upper channel region (and more significantly nearer the interaction region). At the end of the simulation, the breadth of the downward fracture is nearly symmetrical with respect to the stress barrier, although the breadth of the upper half is slightly larger.

### 3.3 Downward Fracturing through a Strong Stress Barrier

For the last case, the same heavy fluid is injected for 2.5 hours at the same TVD, but where the region has a minimum *in-situ* confining stress that follows the *Strong Barrier* profile shown in Figure 1. In this case, there is an increase of 1 MPa over a smaller distance of 5 meters, so that the *local* stress gradient has increased from 0.8 psi/ft to 9.6 psi/ft. Since the local stress gradient (9.6 psi/ft) in this 5-meter formation depth interval is larger than the specific weight of the heavy fluid (1.04 psi/ft), by about an order of magnitude, this 5-meter interval is classified as a *strong stress barrier* according to the definition given above. The shape of the induced fracture, at the end of the simulation, is shown in Figure 4.

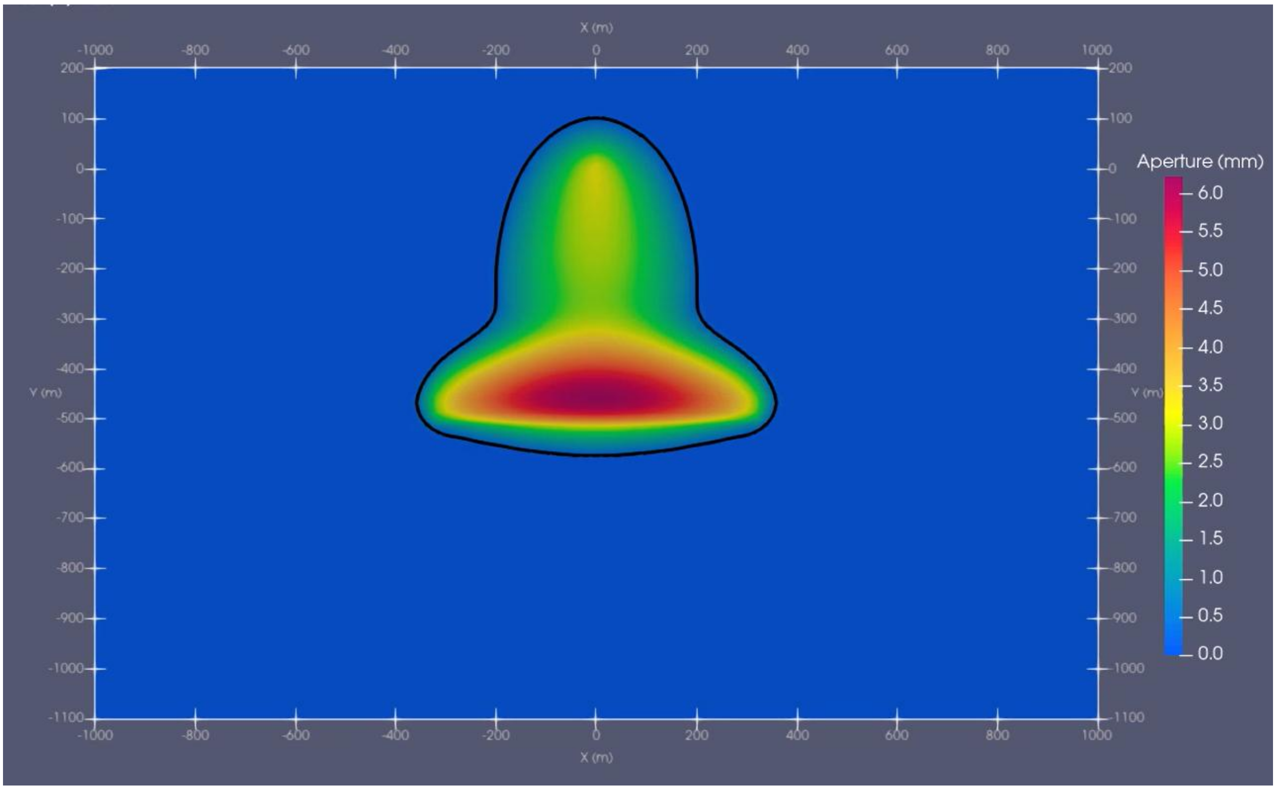


**Figure 4. Shape of the downward fracture that reaches a strong stress barrier.**

At the depths of the strong stress barrier, the local confining stress gradient is larger by about an order of magnitude than the specific weight of the heavy fluid. Thus, the fracture's downward velocity is significantly reduced, and the fracture prefers to grow laterally, again in a height-contained fashion as in the soft barrier case. Note that the barrier decreases the fracture's downward growth while the density of the fluid decreases the fracture's upward growth in the interaction region as it breaks laterally in this region which gives rise to the height-contained behavior. Also noteworthy is that the fracture does penetrate the lower layer below the barrier, but at a very small rate. Much larger injection times need to be made to draw further conclusions on the rate of penetration.

The width of the fracture is largest in the interaction region, attaining twice the magnitude as in the source region. The channel region (or tail) of the fracture, between source and interaction regions, has the next highest widths. Note that the largest widths attained in this Strong Barrier case are doubled compared to those attained in the linear confining stress case. Lastly, the breadth of the downward fracture is non-uniform and is most elongated in the interaction zone near the stress barrier. The fracture growth in the interaction region again influences the fracture breadth in the depth interval containing the channel of the fracture, making the breadth of the channel region larger nearer the interaction zone.

Lastly, if a 10 SG fluid where to be used instead of the 2.4 SG fluid (everything else the same), the 5-meter interval would be classified as a soft barrier as the local stress gradient (9.6 psi/ft) is larger than the specific weight of this much heavier fluid (4.34 psi/ft), but not by an order of magnitude or larger.

### 3.4 Reducing Wellhead Pressure when Stimulating Deep Formations

Besides creating downward propagating fractures, it is essential to highlight that heavy fluids enable pressure reductions at surface in hydraulic stimulations, as well as when operating fractures via Huff-n-Puff strategies, when compared to fracturing with water. For instance, even when injecting a heavy fluid of 1.856 SG into a formation (with parameters as in Table 1) where the minimum *in-situ* confining stress follows the *Linear* profile in Figure 1, that has a gradient of 0.8 psi/ft (equivalent to the specific weight of the fluid), reduces the injection wellhead pressure by half when compared to stimulating with water; note that the fracture is penny-shaped in this heavy fluid case as opposed to a buoyant (or upward elongated) fracture in the case of water. This wellhead pressure decreases further if the 2.4 SG fluid from the previous sections were used instead. Moreover, this pressure reduction becomes further pronounced, and critical, when stimulating super deep formations.

## 4 CONCLUSION

The effect of stress barriers on creating deep downward-oriented fractures has been considered in this short study with simulations carried out using the open-source *PyFrac* solver. First, the results show that in the absence of stress barriers (so that the confining stress gradient is constant), the pumping of heavy fluids, with densities and flowrates seen in the field today, enables creating fractures that can reach 1 km distances below the injection point. Next, if a downward-propagating fracture encounters a soft stress barrier, delineated by both the confining stress gradient and the specific weight of the fracturing fluid, its downward velocity is reduced, and the fracture begins to grow laterally until sufficient mass has accumulated to break through the soft stress barrier and begin a secondary downward growth. This downward fracture can reach a 1 km distance simply by injecting a larger volume of the same dense fluid to account for the fluid contained by the soft stress barrier. Lastly, when the downward-propagating fracture encounters a strong stress barrier, indicated by the larger confining stress gradient but the same heavy fluid as in the previous case, then its downward velocity is reduced even further. In both cases of stress barriers, the breadth of the fracture increases, and significantly increases in the interaction region (near but mainly above the barrier). Also, a height-contained structure is seen to form in this interaction region.

In conclusion, *local confining stress gradients* and the *specific weight* of the fracturing fluid were used in conjunction to classify stress barriers as *soft* or *strong* and this significantly influenced the final shape attained by downward fractures. The results presented here on the fracture shapes of *downward propagating fractures* are complementary to those found for *buoyant (or upward propagating) fractures*. Finally, it was noted that heavy fluids enable reductions in hydraulic fracturing pressure at surface and thus reductions in risks/limitations to hydraulic fracturing equipment; this has merit on its own at current drilling depths and becomes noteworthy when fracturing at deeper depths.

## REFERENCES


Adachi, J., Siebrits, E., Peirce, A. and Desroches, J.: Computer Simulation of Hydraulic Fractures, *Int. J. Rock Mech. Min. Sci.* **44** (2007), 739-757.

Bourne, S., Hindriks, K., Savitski, A. A., Ugueto, G. A., and Wojtaszek, M.: Inference of Induced Fracture Geometries Using Fiber-Optic Distributed Strain Sensing in Hydraulic Fracture Test Site 2, *SPE/AAPG/SEG Unconventional Resources Technology Conference*, Houston, Texas (2021).

Bunger, A.P., Lau, H., Wright, S. and Schmidt, H.: Mechanical Model for Geomechanical Pumped Storage in Horizontal Fluid-Filled Lenses, *Int. J. Numer. Anal. Methods Geomech.* **47**(8), (2023), 1349-1372.

Dahm, T. (2000).: On the Shape and Velocity of Fluid-Filled Fractures in the Earth, *Geophysical Journal International,* 142(1), 181-192 (2000).

Dontsov, E.V. and Peirce, A.P.: Slurry Flow, Gravitational Settling and a Proppant Transport Model for Hydraulic Fractures, *Journal of Fluid Mechanics* **760** (1):567-590 (2014).

Economides, M.J. and Nolte, K.G.: *Reservoir Stimulation*, Wiley, Oxford (2000).

Fei, F., Lu, Y., Bunger, A.P. and Cusini, M.: Experimental and Numerical Study of Hydraulic Fracturing in Enhanced Geothermal Systems (EGS), *Proceedings, 48th Workshop on Geothermal Reservoir Engineering*, Stanford University, Stanford, California (2023).

Fu, W., Damjanac, B., Radakovic-Guzina, Z., Finnila, A., Podgorney, R. and Mclennan, J.: Near-Wellbore DEM Model of Hydraulic Fracture Initiation for Utah FORGE Site, *Proceedings 49th Workshop on Geothermal Reservoir Engineering,* Stanford University, Stanford, California (2024).

Garagash, D.I. and Germanovich, L.N.: Gravity Driven Hydraulic Fracture with Finite Breath, *Proceedings of the Society of Engineering Science 51st Annual Technical Meeting* (ed. A. Bajaj, P. Zavattieri, M. Koslowski and T. Siegmund). Purdue University Libraries Scholarly Publishing Services (2014).

Ghassemi, A. and Kumar, D.: Hydraulic Fracturing in Petroleum and Geothermal Reservoirs with Reference to the Utah FORGE Stimulation, *Proceedings, 48th Workshop on Geothermal Reservoir Engineering,* Stanford University, Stanford, California (2023).

Jeffrey, R.G. and Bunger, A.P.: A Detailed Comparison of Experimental and Numerical Data on Hydraulic Fracture Height Growth Through Stress Contrasts, *SPE J.* 14 (2009): 413-422.

Möri, A. and Lecampion, B.: Three-dimensional Buoyant Hydraulic Fractures: Constant Release from a Point Source, *J. Fluid Mech.* **950**:A12 (2022).

Möri, A., Peruzzo, C., Garagash, D. and Lecampion, B.: How Stress Barriers and Fracture Toughness Heterogeneities Arrest Buoyant Hydraulic Fractures, *Rock Mech Rock Eng* (2024).

Möri, A., Dontsov, E. and Lecampion, B.: Morphology of Buoyancy-Driven Multiple Hydraulic Fractures, *Engineering Fracture Mechanics* **319** (2025).

Peirce, A.P. and Detournay, E.: An Implicit Level Set Method for Modeling Hydraulically Driven Fractures. *Comput. Meth. Appl. Mech. Engng* **197** (2008), 2858-2885.

Peruzzo, C., Lecampion, B. and Zia, H.: Improved Fracture Front Reconstruction in Planar 3D Fluid Driven Fractures Simulation, *14th World Congress on Computational Mechanics (WCCM XIV) and 8th European Congress on Computational Methods in Applied Sciences and Engineering*. International Centre for Numerical Methods in Engineering (2021).

Salimzadeh, S., Hagerup, E.D., Kadeethum, T. and Nick, H.M.: The Effect of Stress Distribution on the Shape and Direction of Hydraulic Fractures in Layered Media, *Engineering Fracture Mechanics* 215: 151-163 (2019).

Salimzadeh, S., Kear, J. and Nick, H.M.: Particle Transport in Fractures: A Common Problem in Enhanced Geothermal Systems and Hydraulic Fractures, *Proceedings World Geothermal Congress 2020,* Reykjavik, Iceland (2020a).

Salimzadeh, S., Zimmerman, R.W. and Khalili, N.: Gravity Hydraulic Fracturing: A Method to Create Self-Driven Fractures, *Geophysical Research Letters* 47, e2020GL087563 (2020b).

Simpkins, D., Rivas, M.A., Eros, M. and Ring, L.: Energy Storage in Deep Hydraulic Fractures: Mathematical Model and Field Validation, *GRC Transactions*, Vol. 47 (2023).

Taisne, B. and Tait, S.: Eruption versus Intrustion ? Arrest of Propagation of Constant Volume, Buoyant, Liquid-filled Cracks in an Elastic, Brittle Host, *J. Geophys. Res.,* 114, B06202 (2009).

Tischner, T., Krug, S., Pechan, E., Hesshaus, A., Jatho, R., Bischoff, M. and Wonik, T., Massive Hydraulic Fracturing in Low Permeable Sedimentary Rock in the GeneSys Project, *Proceedings 38th Workshop on Geothermal Reservoir Engineering,* Stanford University, Stanford, CA (2013).

Tounsi, H., Damjanac, B., Radakovic-Guzina, Z., Fu, W., Finnila, A., Xing, P., Podgorney, R.: A Coupled Hydro-Mechanical Analysis of Impact of DFN on Reservoir Stimulation at FORGE, *Proceedings 50th Workshop on Geothermal Reservoir Engineering*, Stanford University, Stanford, California (2025).

Weertman, J.: Theory of Water-filled Crevasses in Glaciers Applied to Vertical Magma Transport Beneath Oceanic Ridges, *J. Geophys. Res.,* **76**, 1171-1183 (1971).

Weertman, J.: Can a Water-Filled Crevasse Reach the Bottom Surface of a Glacier? *Symposium on the Hydrology of Glaciers,* Cambridge, Sept. 7-13, (1969), Publ. 95, Int. Ass. of Sci. Hydrol., pp. 139-145, (1973).

Zia, H. and Lecampion, B.: PyFrac: A Planar 3D Hydraulic Fracture Simulator, *Comput. Phys. Commun.* **255**:107368 October (2020).